Protein Science (2000), *9*:440–451. Cambridge University Press. Printed in the USA.

The prion domain of yeast Ure2p induces autocatalytic formation of amyloid fibers by a recombinant fusion protein

MARTIN SCHLUMPBERGER,[1,2] HOLGER WILLE,[1,2] MICHAEL A. BALDWIN,[1,2,4] DAREL A. BUTLER,[1,2,5] IRA HERSKOWITZ,[3] AND STANLEY B. PRUSINER[1,2,3]

[1]Institute for Neurodegenerative Diseases, University of California, San Francisco, California 94143
[2]Department of Neurology, University of California, San Francisco, California 94143
[3]Department of Biochemistry and Biophysics, University of California, San Francisco, California 94143
[4]Department of Pharmaceutical Chemistry, University of California, San Francisco, California 94143

(RECEIVED August 24, 1999; FINAL REVISION October 29, 1999; ACCEPTED December 10, 1999)

Abstract

The Ure2 protein from *Saccharomyces cerevisiae* has been proposed to undergo a prion-like autocatalytic conformational change, which leads to inactivation of the protein, thereby generating the [*URE3*] phenotype. The first 65 amino acids, which are dispensable for the cellular function of Ure2p in nitrogen metabolism, are necessary and sufficient for [*URE3*] (Masison & Wickner, 1995), leading to designation of this domain as the Ure2 prion domain (UPD). We expressed both UPD and Ure2 as glutathione-*S*-transferase (GST) fusion proteins in *Escherichia coli* and observed both to be initially soluble. Upon cleavage of GST-UPD by thrombin, the released UPD formed ordered fibrils that displayed amyloid-like characteristics, such as Congo red dye binding and green-gold birefringence. The fibrils exhibited high β-sheet content by Fourier transform infrared spectroscopy. Fiber formation proceeded in an autocatalytic manner. In contrast, the released, full-length Ure2p formed mostly amorphous aggregates; a small amount polymerized into fibrils of uniform size and morphology. Aggregation of Ure2p could be seeded by UPD fibrils. Our results provide biochemical support for the proposal that the [*URE3*] state is caused by a self-propagating inactive form of Ure2p. We also found that the uncleaved GST-UPD fusion protein could polymerize into amyloid fibrils by a strictly autocatalytic mechanism, forcing the GST moiety of the protein to adopt a new, β-sheet-rich conformation. The findings on the GST-UPD fusion protein indicate that the ability of the prion domain to mediate a prion-like conversion process is not specific for or limited to the Ure2p.

Keywords: amyloid; prion; Ure2p; yeast

Prion diseases are a group of progressive neurodegenerative disorders, including Creutzfeldt–Jakob disease in humans, BSE in cattle, and scrapie in sheep, all of which are caused by an abnormal form of the endogenous prion protein (PrP) (reviewed in Aguzzi & Weissmann, 1997; Prusiner, 1998). The term prion was originally defined to describe the proteinaceous infectious particle, which causes these diseases (Prusiner, 1982). In a wider sense, it refers to proteins that have the ability to convert autocatalytically into an abnormal conformation.

Reprint requests to: Stanley B. Prusiner, Institute for Neurodegenerative Diseases, Box 0518, University of California, San Francisco, California 94143-0518.
[5]Present address: Wesley Neurology Clinic, Memphis, Tennessee 38104.

Abbreviations: CD, circular dichroism; FTIR, Fourier transform infrared; GST, glutathione-*S*-transferase; HPLC, high-performance liquid chromatography; PCR, polymerase chain reaction; PMSF, phenylmethylsulfonylfluoride; PrP, prion protein; SDS-PAGE, sodium dodecyl sulfate-polyacrylamide gel electrophoresis; TFA, trifluoracetic acid; ThT, thioflavine T; UPD, Ure2 prion domain; UV, ultraviolet.

Two yeast phenotypes, termed [*URE3*] and [*PSI*], which display a cytosolic dominant pattern of inheritance, were proposed to originate from a mechanism similar to that previously proposed for scrapie (Wickner, 1994) (recent reviews in Wickner & Masison, 1996; Lindquist, 1997; Kushnirov & Ter-Avanesyan, 1998; Liebman & Derkatch, 1999). The prion model provided the first satisfying explanation for a number of puzzling observations that had been reported for the inheritance of these genetic elements. Most notably, they both show fully reversible curability. Second, the [*URE3*] and [*PSI*] phenotypes are indistinguishable from normal, recessive loss-of-function mutations in the genes coding for Ure2p and Sup35p, respectively, and yet depend on the presence of the respective proteins. Third, overexpression of Ure2p or Sup35p leads to a higher rate of spontaneous conversion to [*URE3*] or [*PSI*], respectively.

Several observations provide further support for the hypothesis that [*URE3*] and [*PSI*] are caused by a prion-like mode of inheritance. First, it was shown that both the Ure2p and Sup35p become partially resistant to proteinases in cells displaying the respective

prion phenotype compared to wild-type cells (Masison & Wickner, 1995; Patino et al., 1996; Paushkin et al., 1996). The protease resistance confirms the existence of two structurally different isoforms and is similar to mammalian PrP, which usually acquires protease resistance upon conversion into the disease-causing isoform. Furthermore, both proteins form aggregates upon conversion into the prion form, as shown by fusions to green fluorescent protein (Patino et al., 1996; Edskes et al., 1999), and in the case of [*PSI*], also as assayed by sedimentation (Paushkin et al., 1996). In addition, for [*PSI*], the involvement of different chaperone proteins in appearance, maintenance, and curing of the prion phenotype has been reported (Chernoff et al., 1995; Newnam et al., 1999). These observations strengthen the hypothesis that [*PSI*] is generated by a conformational change of Sup35p.

Both the Ure2 and Sup35 proteins contain short N-terminal domains, which consist of mainly polar, uncharged amino acids, and are fully dispensable for their respective cellular functions in nitrogen metabolism and termination of translation (Coschigano & Magasanik, 1991; Ter-Avanesyan et al., 1993). These domains, on the other hand, are necessary for the appearance and maintenance of the prion phenotype and are also sufficient to propagate the prion determinant. In the case of Ure2p, the first 65 amino acids have been shown to function as a prion domain (Masison & Wickner, 1995), although the region consisting of mainly polar residues extends further to about 89 residues, almost 50% of which are either asparagine or glutamine.

Amyloids are deposits of ordered aggregates, rich in β-sheet, which occur in a number of human diseases, including the prion diseases (Prusiner et al., 1983; Sunde & Blake, 1998). The regular arrangement of cross β-sheet structures leads to a characteristic green–gold birefringence upon binding of Congo red dye. Amino-terminal portions of Sup35p have been expressed and purified from *Escherichia coli*, and shown to form highly ordered fibrous structures that show all the characteristics of amyloid (Glover et al., 1997; King et al., 1997). Fiber formation from solutions of denatured protein can be seeded by preformed fibers or extracts from [*PSI*], but not wild-type yeast strains, and proceeds in an autocatalytic manner. This behavior could account for the appearance and inheritance of [*PSI*] in yeast. Indeed, one study shows that Sup35p in yeast extracts can be converted to an insoluble, partially protease-resistant form by mixing with extracts from a [*PSI*] strain (Paushkin et al., 1997). Mutagenesis studies (DePace et al., 1998) show that glutamine and asparagine residues close to the N-terminus of the Sup35 prion domain are crucial for propagation of [*PSI*] and amyloid formation in vitro. A formal proof, however, that amyloid formation occurs inside yeast cells or that aggregated Sup35 protein can infect cells to make them [*PSI*] remains to be shown.

Two recent studies (Taylor et al., 1999; Thual et al., 1999) demonstrate the formation of amyloid-like fibrils by Ure2p or its prion domain. Taylor et al. obtained fibers formed by a synthetic peptide comprising the first 65 residues of Ure2p. These fibers could, in turn, bind roughly stoichiometric amounts of native Ure2p from yeast, which caused the bound Ure2p to become partially resistant to proteinase K. Upon prolonged incubation, these mixed fibers could precipitate more Ure2p, again rendering it partially proteinase resistant. Thual et al. purified Ure2p expressed in *E. coli* and found the protein to oligomerize in a concentration-dependent manner. Upon prolonged storage or a shift to lower pH, the material formed short fibrils resembling amyloids, which also exhibited partial resistance to treatment with different proteases.

In the study reported here, we expressed and purified fusion proteins of the N-terminal 69 residues (UPD) and the full-length Ure2 protein with glutathione-*S*-transferase (GST). Free UPD formed amyloid-like fibrils in an autocatalytic process that could be seeded by preformed fibers. Surprisingly, the UPD-GST fusion protein also formed amyloid fibers autocatalytically. FTIR spectroscopy suggests formation of extensive new β-sheet structures, not only in the UPD but also in the GST moiety of the protein. These findings indicate that the prion-forming activity of the N-terminal domain of Ure2p does not require specific interactions with the C-terminal portion of the protein. Free Ure2p aggregated slowly with little fiber formation, but seeding with UPD fibers accelerated the process, leading to more protease-resistant aggregates.

Results

Purification of recombinant proteins

We chose to use GST fusions for expression and purification because they allow for efficient one-step purification. This method also permits release of the protein of interest from the GST moiety by selective proteolytic cleavage with the protease thrombin. Furthermore, GST fusion proteins often retain the native conformation and function of the fused protein, and are frequently soluble in *E. coli*, even at high expression levels. GST-Ure2 as well as GST-UPD fusion proteins were found in the supernatant fractions when bacterial cell extracts were clarified by centrifugation at $12{,}000 \times g$ for 15 min. From such lysates, however, GST-UPD precipitated highly selectively and almost quantitatively within 24 h.

Purified GST-UPD remained soluble at concentrations below 3 mg/mL, but showed a strong tendency to aggregate at higher concentrations. Protein solutions with concentrations above 5 mg/mL eventually formed a solid gelatinous mass. In contrast, the purified GST-Ure2 fusion protein showed little tendency to form insoluble aggregates, although analysis by light scattering indicated formation of various oligomeric forms.

Formation of UPD amyloid fibers

Cleavage of the GST-UPD protein invariably resulted in the formation of macroscopic aggregates that precipitated within a few hours. The precipitate contained not only UPD but also almost all of the GST protein.

The UPD fragment demonstrated abnormal migration and staining behavior on SDS-PAGE; we were unable to detect UPD on SDS-PAGE with standard Coomassie blue or silver staining procedures, even on highly overloaded gels. A polyclonal rabbit antiserum detected UPD on Western blots only when samples for SDS-PAGE were prepared in the presence of 6 M urea, and when an additional denaturation step with NaOH was introduced after transfer to the nitrocellulose membrane (Fig. 1; see Materials and methods).

Second, UPD always appeared on Western blots as a double band with apparent molecular weights of about 12 and 15 kDa, instead of 7.5 kDa, as predicted from the amino acid sequence. To ensure that the formation of two bands was not due to alternate cleavage by the thrombin protease, the products from cleavage of the fusion protein were separated by reversed-phase HPLC, using a linear gradient of aqueous 0.1% TFA and 0.08% TFA in aceto-

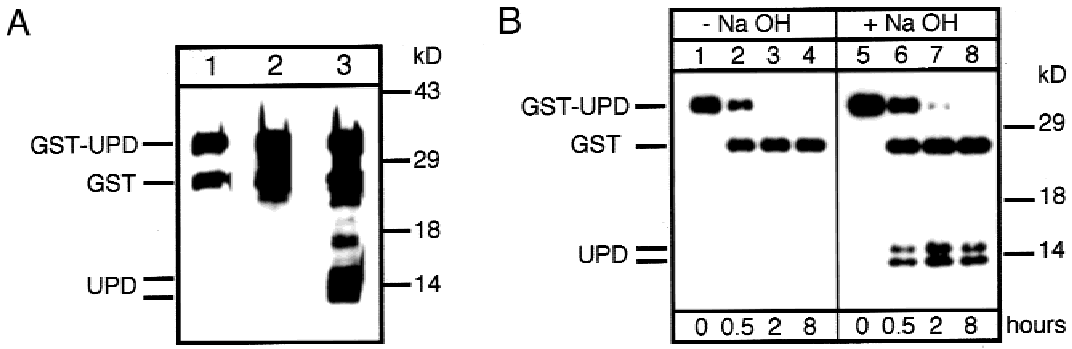

Fig. 1. Detection of UPD on Western blots and analysis by mass spectrometry. **A:** Products of partial cleavage of GST-UPD by thrombin. Lane 1 was developed according to standard protocol, lane 2 with an additional 30 min denaturation step in 6 M guanidine hydrochloride after transfer, and lane 3, denaturation with 0.2 M NaOH. Despite the high protein load, UPD is detected only if NaOH denaturation is used. **B:** Kinetics of GST-UPD cleavage by thrombin. Left panel, without NaOH denaturation, the UPD is not detected; right panel, with alkali treatment, two additional bands are visible. Cleavage of GST-UPD is essentially complete after 2 h. **C:** The reversed-phase HPLC chromatogram of the products of the cleavage of the GST-UPD fusion protein. **D:** MALDI-MS spectrum of the HPLC peak eluting at 22 min, identified in **C** as "UPD." **E:** ESI-MS spectrum of the same fraction as in **D**. **F:** The molecular weight profile obtained by deconvolution of the ESI-MS spectrum in **E**. (*Figure continues on facing page.*)

nitrile. The UV chromatogram (Fig. 1C) gave a sharp isolated peak that eluted after 22 min, followed by a series of poorly resolved components that eluted between 45 and 50 min. Fractions were collected for analysis by mass spectrometry. An initial rapid survey was carried out using matrix-assisted laser desorption/ionization mass spectrometry (MALDI-MS) without internal mass calibration, after which more accurate measurements were made on specific fractions of interest using electrospray ionization mass spectrometry (ESI-MS). MALDI-MS for the fraction eluting at 22 min showed singly and doubly charged ions (Fig. 1D), giving an average molecular weight of 7,620.1 Da. Although the mass scale of the mass spectrometer was uncalibrated, the result was consistent with the UPD fragment of calculated mass 7,633.8. The unresolved peaks that eluted later were seen to contain the intact fusion protein, the cleaved GST fragment, and a number of other cleavage products.

The 22 min fraction believed to contain the UPD fragment was infused into the ESI mass spectrometer. As is typical of ESI-MS, the mass spectrum showed a series of peaks corresponding to the addition of multiple protons, in this case between 4 and 7, with the strongest signal for the addition of 5 (Fig. 1E). The data were smoothed and deconvoluted to convert from mass/charge (m/z) to molecular mass using software provided with the mass spectrometer, giving a single peak of molecular weight 7,633.8 Da (Fig. 1F). This was identical to the calculated value for UPD, which confirmed the identity of this species.

The same double band was also observed when the same UPD fragment was expressed in yeast (data not shown). In some cases, a ladder of bands with decreasing electrophoretic mobility was observed. Therefore, we conclude that the UPD fragment forms dimers or higher oligomers, even under the conditions of standard SDS-PAGE, and that this process interferes with immunological detection under standard procedures.

Analysis of the aggregates by negative stain electron microscopy showed that it contained regular fibrous structures, as well as some amorphous aggregates. To remove co-precipitating GST, sucrose gradient centrifugation of the cleavage products was performed. While the amorphous aggregates formed by the GST protein were retained in the upper, low-density fractions of the gradient, all of the UPD protein migrated into the bottom fraction (Fig. 2). Western blot analysis and ultrastructural examination of the different fractions confirmed that the fibrous structures were exclusively formed by UPD. Electron microscopy of the purified UPD confirmed a strong resemblance of the UPD fibers to amyloids (Fig. 3A).

To determine whether the fibers formed by UPD behave like typical amyloid, Congo red dye binding assays were performed. UPD fibers not only bound the dye, but also showed strong green–gold birefringence in polarized light (Fig. 4A,D), characteristic of the highly ordered, cross-β-sheet structure typical of amyloids. To analyze further the secondary structure in these fibers, FTIR spectroscopy was performed (Table 1). The results confirm a β-sheet content of about 50%, comparable to that found in other amyloids.

In all experiments described here, aggregates formed macroscopic particles, making analysis by light scattering or turbidity measurements highly inaccurate. Therefore, to follow the kinetics of fiber formation, we used the fluorescent dye thioflavine T (ThT). The dye binds to proteins with ordered β-sheet structure, leading to a new absorption maximum at 450 nm and fluorescence at 482 nm (LeVine, 1993). Because there is practically no fluorescence at 482 nm in the absence of β-sheet-rich, ordered aggregates, the assay is highly specific for amyloid formation with very little background.

When GST-UPD was cleaved at a concentration of 1 mg/mL (30 μM) by thrombin, ThT fluorescence showed no significant increase within the first 2 h (Fig. 5). However, if cleavage was performed in the presence of 2% (w/w) preformed UPD fibers, cleavage and polymerization into β-sheet–rich aggregates proceeded in parallel. Therefore, fiber formation by UPD is an autocatalytic process. When the cleavage reaction was performed at lower protein concentrations, the lag phase was prolonged. At 0.3 mg/mL (9 μM), it increased from 2 to 3 h to about 4 to 5 h. Kinetics of the seeded polymerization was slowed down as well, and the final fluorescence intensity was lower than at higher concentration.

Amyloid fiber formation by GST-UPD

In aggregates spontaneously formed by GST-UPD at higher concentrations (above 3 mg/mL or 90 μM), negative stain electron

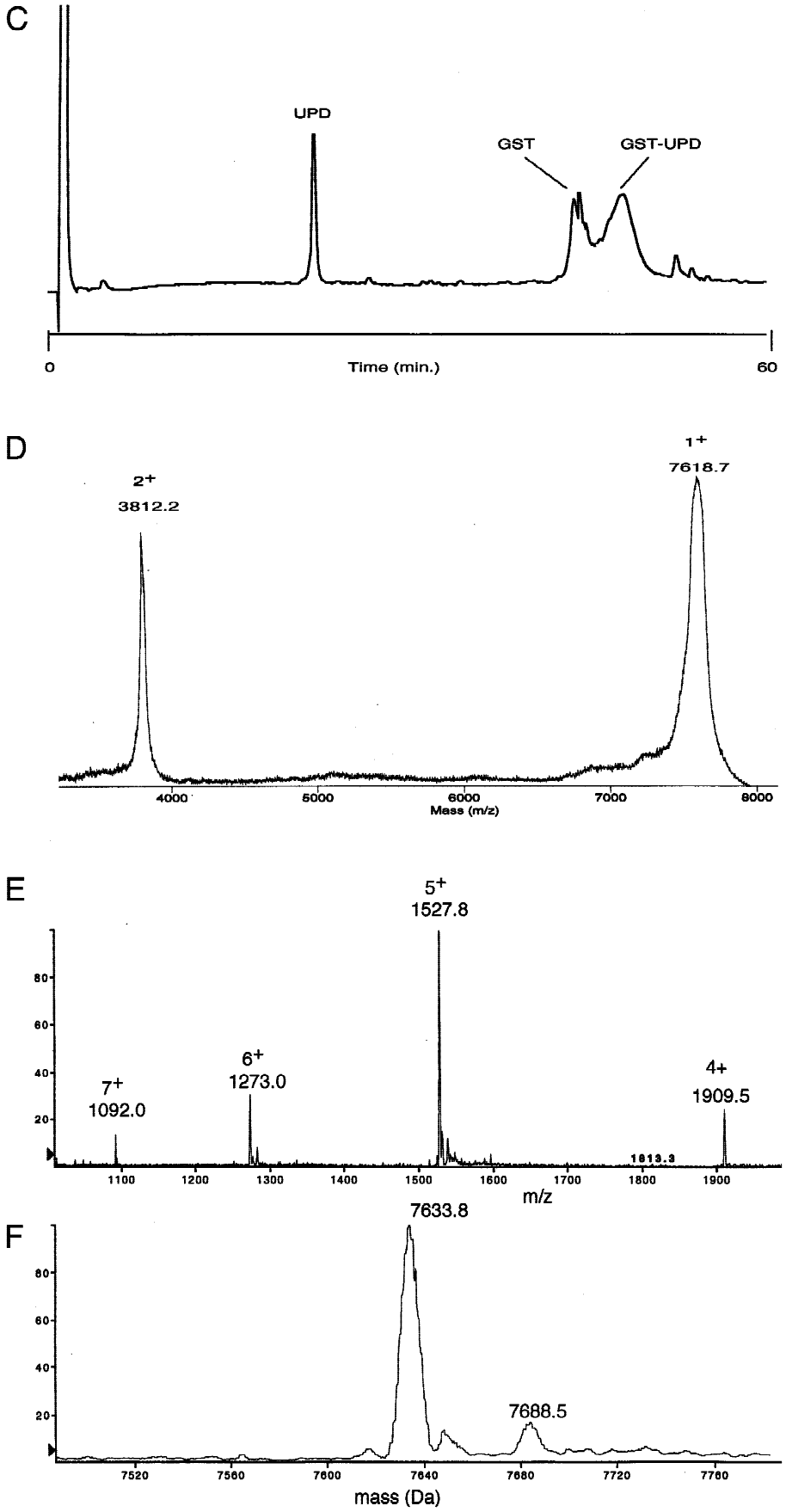

Fig. 1. *Continued.*

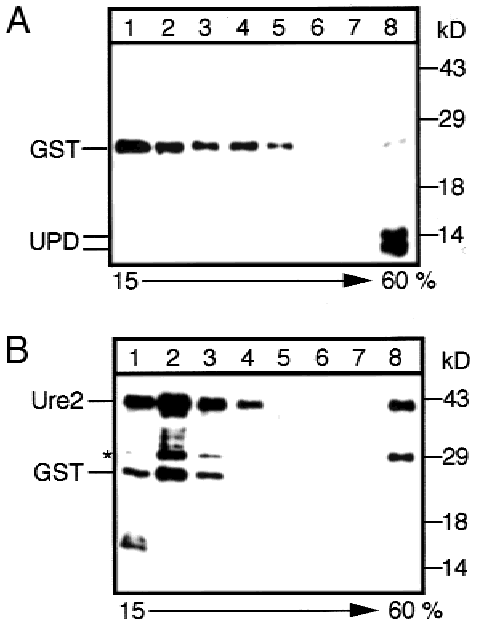

Fig. 2. Separation of ordered and amorphous aggregates on sucrose gradients. Samples for Western blotting were thrombin cleavage products of GST-UPD or GST-Ure2 after fractionation on continuous 15 to 60% sucrose gradients. Amorphous aggregates formed by coprecipitating GST are separated away from more ordered aggregates formed by the UPD or Ure2p parts of the fusion proteins. **A:** UPD segregates quantitatively into the pellet fraction of the gradients. The material recovered from that fraction shows fibers with typical amyloid characteristics. **B:** Under the same conditions, only a minor amount of Ure2p is recovered in the highest density fraction of the gradient, indicating inefficient fiber formation. This is in agreement with electron microscopic observations of mostly amorphous aggregates formed upon GST-Ure2 cleavage. The asterisk indicates a partial degradation product of GST-Ure2.

microscopy revealed unexpectedly high amounts of amyloid-like fibers (Fig. 3B). In sucrose gradients, the aggregated protein was quantitatively recovered in the pellet fraction, indicating efficient conversion into aggregates with high density. These samples also displayed increased resistance to proteinase K digestion (Fig. 6A). The entire fusion protein became partially protease resistant, although smaller fragments in the size range observed for UPD (Fig. 1B) persisted for longer incubation times. The aggregates also bound Congo red dye and showed birefringence in polarized light (Fig. 4B,E). Similar fibers were also found in aggregates that formed after prolonged incubation at room temperature in bacterial extracts from cells expressing GST-UPD (data not shown).

CD spectroscopy was performed on the soluble form of GST-UPD (Fig. 6B) as well as GST itself. Structural data on *Schistosoma* GST obtained by X-ray crystallography (McTigue et al., 1995) show an α-helical content of 46% and β-sheet content of 8%. Similar numbers (42/17%) were obtained from CD spectroscopy. The α-helical content of soluble GST-UPD was about 33% and the β-sheet content about 11%. Comparison of the data indicates that practically all these secondary structural elements are contributed by the GST moiety of the protein, suggesting that the UPD portion is largely unstructured. Although CD spectra of the aggregated form of GST-UPD were qualitatively different from those of the soluble protein, poor quality of the data obtained at wavelengths below 200 nm did not allow a good estimate of secondary structure. Because CD spectroscopy is known to be difficult with aggregated proteins and does not quantitate β-sheet accurately, FTIR spectroscopy was performed on the soluble and fibrous forms of the protein (Fig. 6C; Table 1). FTIR measurements on soluble GST-UPD were complicated by the tendency of the protein to aggregate upon reconstitution in D_2O. Also, the α-helical content of soluble GST-UPD appears to be partially misinterpreted due to a slight shift in absorption to higher wave num-

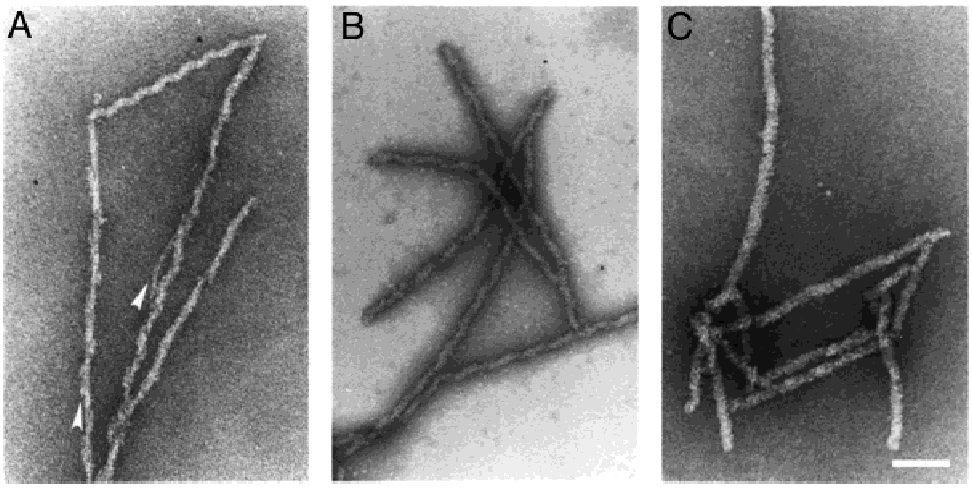

Fig. 3. Negative stain electron microscopy of fibers obtained by sucrose gradient centrifugation. **A:** Fibers formed by UPD show typical amyloid-like substructure, with a diameter of about 11 nm ± 4 nm (range 5–17 nm), consisting of thin protofilaments with about 5 nm width (arrowheads). **B:** GST-UPD forms slightly thicker fibers with a diameter of 14 nm ± 2 nm (range 10–16 nm). **C:** Ure2p fibers are thicker than those formed by UPD or GST-UPD (22 nm ± 3 nm in diameter, range 17–28 nm) and tend to be shorter and have a fuzzier appearance. This indicates that the C-terminal domain of the protein takes on a less-ordered structure in the fibers, with a core probably being formed by the prion domain. Stained with 2% ammonium molybdate. Bar equals 100 nm.

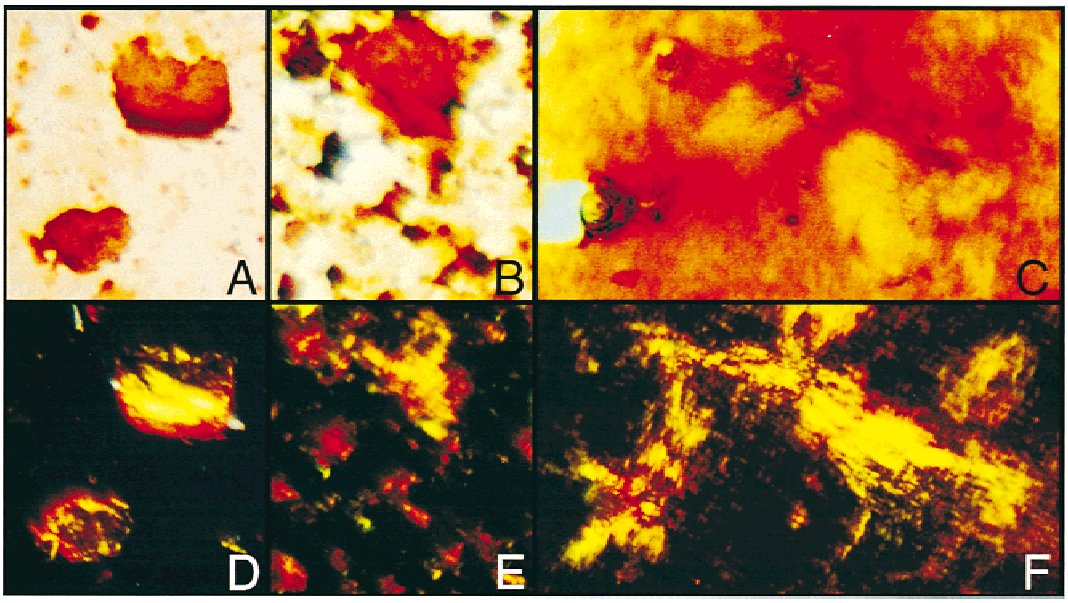

Fig. 4. Congo red staining and birefringence. **A–C:** Staining of ordered aggregates with Congo red dye in bright field. **D–F:** In polarized light (dark field) the stained aggregates shown in **A–C** all exhibit strong green–gold birefringence. All aggregates were purified by sucrose gradient centrifugation. **A,D:** UPD. **B,E:** Ure2. **C,F:** GST-UPD.

bers. It is known that α-helices do not give a highly characteristic signature in FTIR spectra. Samples showing little precipitation upon reconstitution indicated β-sheet content of about 10%, in good agreement with the data obtained by CD. For GST-UPD fibers, a β-sheet content of 44–49% was observed, corresponding to about 130–145 amino acids out of 295. With 8% β-sheet in GST (19 residues) and UPD amounting to 69 amino acids in GST-UPD, at least 61 residues (27%) in the GST moiety acquire β-sheet conformation upon conversion into the amyloid form. Comparison of the known α-helical content of GST and the data obtained by CD spectroscopy for soluble GST-UPD, with the extent of β-sheet formation determined by FTIR spectroscopy, therefore clearly indicates a substantial change in secondary structure not only in the UPD but also in the GST part of the molecule upon fiber formation.

To examine whether GST-UPD supports autocatalytic polymerization, soluble fusion protein was diluted to 1 mg/mL (30 μM) and incubated at room temperature under constant slow rotation in the presence and absence of preformed GST-UPD aggregates. At regular time intervals, samples were taken, diluted into ThT containing buffer, and fluorescence intensities determined. The measurements show that GST-UPD at low concentrations remains soluble in the absence of seed, whereas addition of fibers leads to autocatalytic propagation of the fibrous state and formation of

Table 1. *Secondary structure content estimated from FTIR spectroscopy*[a]

	α-Helix (%)	β-Sheet (%)	Other (%)
UPD fibers	14–24	45–67	19–32
Ure2 fibers	29	40–41	30–31
GST-UPD soluble[b]	16–31	10–34	30–74
GST-UPD fibers	21–27	44–49	24–35

[a] Percentages shown give the range over three independent experiments.
[b] Soluble GST-UPD partially aggregated upon reconstitution in D_2O. The experiment in which most of the protein stayed soluble indicated a β-sheet content of 10%, in good agreement with data obtained from CD spectroscopy. Higher values most likely reflect partial aggregation of the sample.

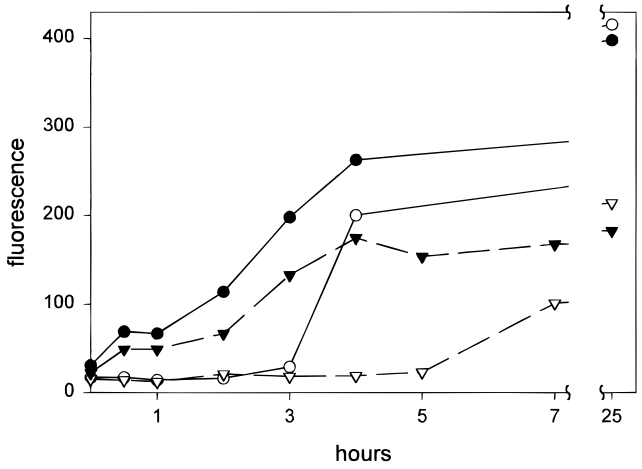

Fig. 5. Autocatalysis of fiber formation by UPD. Thrombin cleavage of GST-UPD was performed at 1 mg/mL (circles) or 0.3 mg/m: (triangles) in the presence (filled symbols) or absence (open symbols) of 2% preformed fibers as seed. Formation of ordered β-sheet structure was followed by measuring ThT fluorescence at 482 nm (excitation wavelength: 450 nm). In the absence of seed, at 1 mg/mL a lag phase of 2–3 h is observed. At 0.3 mg/mL the lag phase is about 5 h. Due to variance in absolute fluorescence intensity between experiments, data shown are from one representative experiment. The length of the lag phase was highly reproducible.

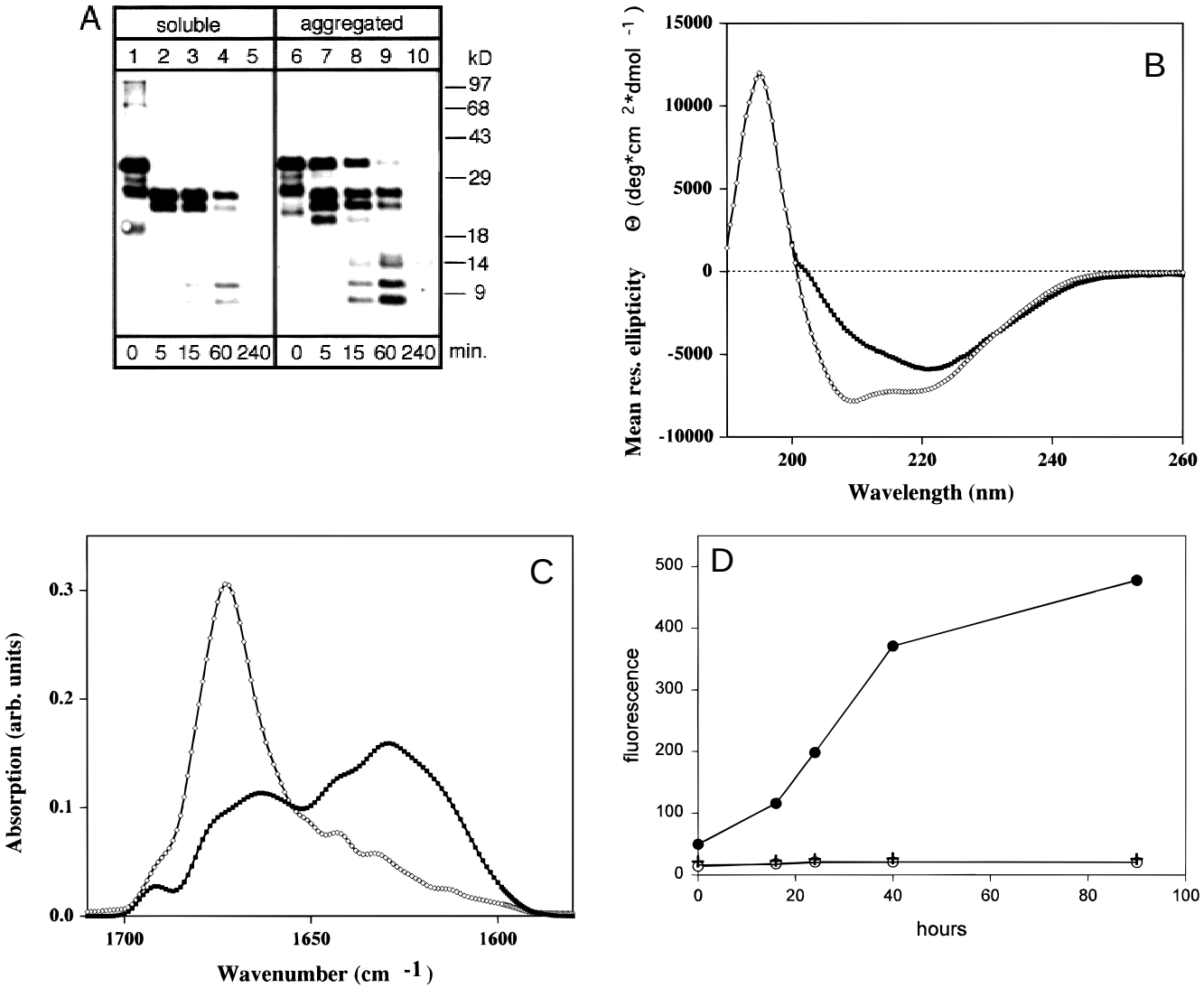

Fig. 6. Fiber formation by GST-UPD. **A:** Western blot showing proteinase K resistance of soluble and aggregated GST-UPD. The soluble full-length protein is digested within the first 5 min, although a fragment of roughly the size of GST persists for up to 1 h. In the aggregated state, small amounts of the full-length protein survive up to 1 h; a 24–27 kDa band, a pair of bands around 14 kDa reminiscent of the signature of UPD (compare with Fig. 1B), and smaller fragments are even more resistant. **B:** CD spectra of soluble (open diamonds) and aggregated (filled squares) GST-UPD. **C:** FTIR spectra of soluble (open diamonds) and aggregated (filled squares) GST-UPD. The increase in absorption between 1,600 and 1,650 cm^{-1} indicates an increase in β-sheet content upon aggregation. Partially aggregated samples yielded intermediate spectra. **D:** Incubation of GST-UPD with preformed fibers (filled circles) leads to a dramatic increase in ThT fluorescence at 482 nm, indicating efficient formation of highly ordered β-sheet rich aggregates. On contrast, virtually no change was observed when the protein was incubated in the absence of seed (open circles) or in the presence of supernatant from aggregated GST-UPD after passage through a 300 kDa filter (crosses).

macroscopic aggregates rich in ordered β-sheet (Fig. 6D). When partially aggregated solutions of GST-UPD were filtered through a 300 kDa filter, the protein in the filtrate lost the seeding activity, indicating that the converting species is larger than 300 kDa and probably a complex of at least 10 molecules. Polymerization of GST-UPD could also be seeded with fibers consisting of UPD alone (data not shown).

To learn more about the mechanism of conversion, the influence of different chemicals was examined. If partial unfolding of the GST moiety were rate limiting, glycerol could be expected to stabilize the native conformation, thereby slowing down polymerization. Similarly, low concentrations of urea might accelerate it. Arginine or asparagine might interfere with the interactions between protein monomers. However, no significant effects of any of these chemicals were observed, with the exception that urea at concentrations of 1 M or higher abolished the seeding activity completely (data not shown). Fiber formation led to a reduction of the GST enzymatic activity, but with significantly slower kinetics than amyloid formation (as measured by ThT fluorescence). Addition of the competitive GST inhibitors S-hexyl-glutathione and praziquantel had no effect on the polymerization. The glutathione binding site is located close to the N-terminus of GST, while amyloid formation is presumably initiated by the UPD, at the C-terminus of GST.

Fiber formation by Ure2p

Although small amounts of GST-Ure2p eventually precipitated from solutions of the purified protein after prolonged storage at 4 °C as well as from bacterial lysates, no fiber formation was observed. Upon cleavage with thrombin, the cleavage products formed a visible precipitate only after more than 10 h, while the cleavage itself was virtually complete in about 2 to 3 h. Under these conditions, only a low amount of fibers (Fig. 3C) was formed, aside from mostly amorphous aggregates. Some experiments produced no detectable fibers at all. In sucrose gradient centrifugation, the majority of the Ure2p was retained in the upper fractions (Fig. 2).

Seeding with UPD fibers accelerated the aggregation substantially. When thrombin cleavage of GST-Ure2p was performed in the presence of 3% UPD fibers (corresponding to a molar ratio of about 1:4), aggregates were clearly visible after 60–90 min, indicating that release of the Ure2p was immediately followed by incorporation into aggregates. Although the thioflavine fluorescence assay indicated the formation of at least some ordered, crossed β-sheet aggregates (Fig. 7A), electron microscopic examination of the reaction products showed little increase in the amount of regular fibers being formed. Analysis by sucrose gradient centrifugation and proteinase K digestion (Fig. 7B) showed variable amounts of high density, proteinase-resistant material after 24 h. The most persistent fragments formed a similar pattern to that observed for UPD (Fig. 1B). The amount of Ure2p recovered in the bottom fraction of the sucrose gradient varied from 10% to >90%.

Our observations demonstrate that the formation of aggregates by Ure2p can proceed in an autocatalytic manner, which could explain the [*URE3*] prion phenotype in yeast. Under these conditions, the seed can apparently catalyze formation of dense, highly ordered structures as well as more amorphous aggregates. Therefore, we observed great variability in the outcome of the reaction between individual experiments using different preparations of seed and fusion protein.

In the cellular environment, formation of amorphous aggregates is prevented by chaperone proteins and high concentrations of small molecules (Tatzelt et al., 1996). Therefore, the cleavage and aggregation experiment was repeated in the presence of 20% glycerol. In the absence of seed, glycerol delayed aggregation of Ure2p substantially but had little effect on the amount of dense, protease-resistant aggregates being formed. In the presence of seed, glycerol affected the increase in ThT fluorescence only marginally (Fig. 7A), while it typically led to more proteinase-resistant dense aggregates (Fig. 7B), albeit with slower kinetics.

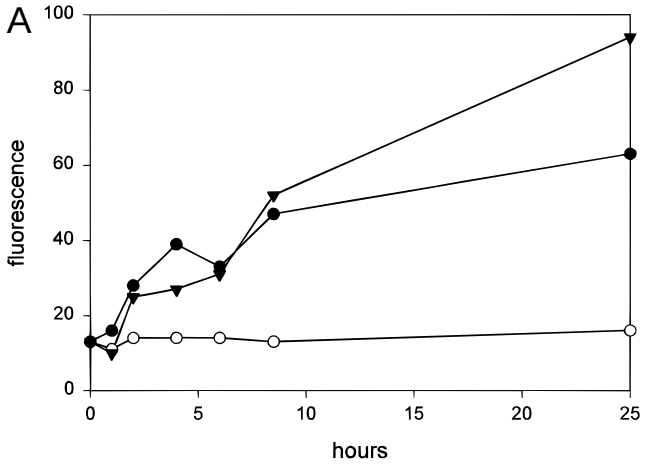

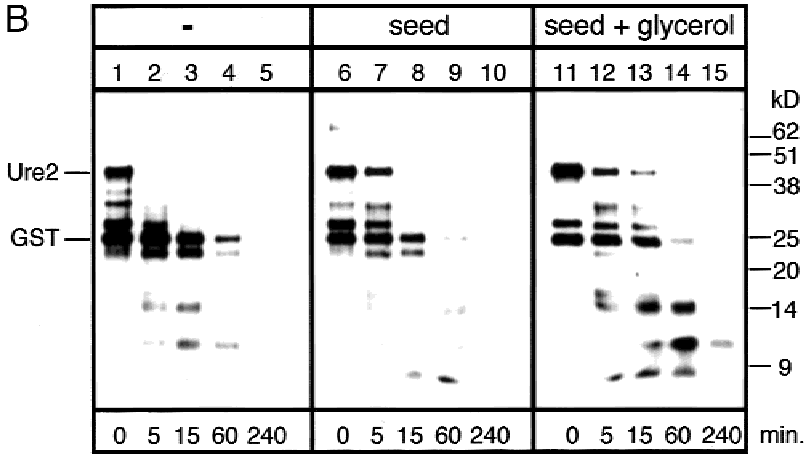

Fig. 7. Fiber formation by Ure2p. **A:** Thrombin cleavage of GST-Ure2 and aggregation assayed by ThT fluorescence. In the absence of seed (open circles), a slight increase due to nonspecific aggregation and light scattering can be seen after prolonged incubation but without a maximum at 482 nm. In the presence of 3% UPD fibrils (filled circles), a significant increase in fluorescence with a clear maximum around 482 nm is observed. Incubation in the presence of 3% UPD fibrils and 20% glycerol (filled triangles) causes only slight changes in the time course or fluorescence intensity compared to incubation with seed in the absence of glycerol. Data are from one representative experiment. For clarity, the contribution of the seed (about 40 arbitrary units) was deducted from measurements of the seeded reactions. **B:** Western blot showing proteinase K sensitivity of GST-Ure2 thrombin cleavage products after 40 h incubation at room temperature. Left panel, incubation in TBS-TX buffer without seed. No Ure2p is found after 5 min of proteinase exposure, while GST persists for up to 1 h. In the presence of 3% UPD fibers as seed (middle panel), full-length Ure2p becomes more protease resistant. In the presence of seed and 20% glycerol, protease resistance becomes more pronounced, and the double band around 14 kDa, which seems to be characteristic for UPD fibers (compare with Fig. 1B), appears after 15–60 min of incubation.

Discussion

The yeast prions [*URE3*] and [*PSI*] are important model systems that allow the study of protein folding events that are thought to resemble those involved in some human diseases. Regular linear aggregates that form spontaneously by the prion domain of yeast Ure2p display a morphology strikingly similar to fibers found in all amyloid diseases (Cohen et al., 1982; Sunde & Blake, 1998). They show typical characteristics of amyloid, such as a high β-sheet content, and bind the dyes thioflavine T and Congo red, leading to characteristic fluorescence and birefringence, respectively. Formation of amyloid fibers by UPD alone or mediated by the Ure2 prion domain in a longer protein proceeds in an autocatalytic manner. This mechanism of autocatalytic polymerization could explain the propagation of the [*URE3*] prion phenotype in yeast. It is also consistent with the formation of insoluble, proteinase-resistant aggregates by Ure2p in yeast strains with the [*URE3*] phenotype (Masison & Wickner, 1995).

Amyloid formation by GST-UPD

Surprisingly, the recombinant GST-UPD fusion protein in vitro shows all the characteristics expected from a prion protein in vivo; it is stable in a soluble, active form for a prolonged time but can be efficiently converted into an insoluble species autocatalytically. This behavior demonstrates that the fusion of the Ure2 prion domain to a heterologous protein can be sufficient to confer prion-like behavior, at least in vitro. It has been suggested (Masison et al., 1997) that Ure2p is inactivated in [*URE3*] strains by a specific interaction of the prion domain with the C-terminal regulatory domain. Our studies on the GST-UPD fusion protein demonstrate that such an interaction is not necessary for autocatalytic polymerization induced by the prion domain. Because Ure2p shows homology to some GST proteins (Coschigano & Magasanik, 1991), it could be argued that the potential for interaction with UPD is conserved in the GST-UPD fusion protein. However, pairwise alignment of the *Schistosoma* GST with the C-terminus of Ure2p shows less than 20% sequence identity. Because GST contains no domain that shows any similarity to the UPD, the conservation of such a specific interaction appears rather unlikely, although possible similarities in tertiary structure between Ure2p and GST might play a role in fiber formation. It is noteworthy, however, that the fusion protein described here carries UPD on the C-terminus, whereas it is on the N-terminus of Ure2p. Finally, a fusion protein between GST and the prion domain of Sup35p, which does not show any homology to GST, can also form amyloid fibers (M.M. Balbirnie & D. Eisenberg, pers. comm., 1999). It is possible that a specific interaction between UPD and the functional domain is involved in the inactivation of Ure2p in [*URE3*] strains, but the loss of function could simply follow from partial refolding and aggregation of the protein.

Three separate lines of evidence indicate that β-sheet formation and polymerization into ordered fibrils by the recombinant GST-UPD protein is initiated by the prion domain and extends into the GST moiety. First, limited digestion with proteinase K showed that the full-length fusion protein acquired partial resistance. Second, the aggregated form of the fusion protein was fully resistant to thrombin cleavage, indicating that the region containing the cleavage site becomes inaccessible to the protease. Third, spectroscopic data on the soluble and aggregated forms of GST-UPD argue for a substantial increase in β-sheet structure in the GST moiety. The core structure of the GST-UPD fibers appears to be formed by UPD because it shows the greatest propensity for fiber formation, the highest resistance to protease digestion, and it can seed amyloid formation by GST-UPD and Ure2p. Therefore, the newly formed β-sheet structures in GST-UPD are most likely induced by the extension of strands from UPD into the GST moiety. Existing β-sheet regions in native GST are located near the N-terminus of the protein (McTigue et al., 1995). The requirement for a conformational change within the GST moiety could also explain why fiber formation by GST-UPD proceeds much slower than fiber formation by UPD alone.

Inhibition of amyloid formation

An important question raised by our experiments is why the fusion of GST to UPD inhibits the formation of aggregates, whereas free UPD polymerizes spontaneously. Two observations indicate that the inhibition is likely to be due to steric hindrance by the GST moiety. First, in experiments where the cleavage of GST-UPD was not quantitative, all the uncleaved fusion protein was found in the high-density fraction after sucrose gradient centrifugation, indicating that minor amounts of uncleaved GST-UPD can be incorporated into UPD fibers without undergoing a slow conformational change. Second, when the FLAG epitope was introduced into the fusion protein between the GST and UPD moieties, the tendency of the fusion protein to aggregate increased substantially, despite the highly hydrophilic nature of the FLAG sequence. Apparently, the additional eight amino acids act as a spacer, decreasing the steric constraints on fiber formation.

Polymerization of Ure2p

In our studies, autocatalytic polymerization of full-length Ure2p into amyloid fibers proceeded only with low efficiency. Apparently, ordered polymerization competes with the formation of less ordered aggregates. Nonspecific aggregation of Ure2p at physiological buffer conditions has also been reported by other groups (Perrett et al., 1999; Taylor et al., 1999), and the protein is often partially insoluble even in yeast strains not showing the prion phenotype (M. Schlumpberger, unpubl. obs.). On the other hand, the UPD-GST fusion was efficiently converted into fibers in vitro, but we found no indication of polymerization in yeast. Because in vivo chaperone proteins and high concentrations of small molecules are involved in keeping proteins in their native states, it is possible that conformational instability of Ure2p and the tendency to aggregate are a prerequisite for conversion to the prion state in yeast. It is noteworthy that aggregation of Ure2p proceeded with slower kinetics than polymerization of UPD alone, but faster than GST-UPD, indicating that GST has a stronger inhibitory effect on fiber formation than the C-terminal domain of Ure2p. These observations are also consistent with a recent study (Perrett et al., 1999) that demonstrated that the presence or absence of the prion domain has no effect on folding or dimerization of the C-terminal part of Ure2p, although it does increase its propensity to precipitate from solutions. The study also shows that the UPD is mostly unstructured in soluble Ure2p, a result consistent with our findings on UPD in soluble GST-UPD.

Our results are in clear contrast to those of Thual et al. (1999), who reported substantially lower proteinase resistance (at 2.4 μg/mL compared to 25 μg/mL proteinase K in our experiments) and found no indication of increased resistance to limited proteolysis

by the prion domain. In the in vitro translation experiments, protein concentration was most likely too low for fiber formation by the N-terminal fragment. Also, the Coomassie staining procedure employed to obtain proteinase digestion profiles of the full-length Ure2p failed to detect aggregated UPD in our experiments. It seems likely, therefore, that protease-resistant fragments containing the Ure2p N-terminus were not detected by Thual et al. because of the staining procedure used. The experiments presented here demonstrate that fiber formation is initiated by UPD and fragments containing the prion domain show the highest β-sheet content and the highest resistance to proteinase K digestion.

Possible mechanisms of [URE3] formation

Two models have been proposed for the mechanism by which the mammalian prion protein is converted from the normal, cellular form into the abnormal, pathogenic scrapie isoform. According to the template-assistance model (Cohen & Prusiner, 1998), conversion occurs when the cellular and scrapie variants of the protein form a mixed dimer or oligomer, followed by release of a new molecule of the scrapie form. The seeded nucleation model (Gajdusek, 1988; Jarrett & Lansbury, 1993) proposes that the converting species is a linear amyloid crystal, and that the conformational change occurs when a new monomer is incorporated into the fiber. The findings presented in this study clearly favor a nucleation-dependent mechanism in which the aggregated form is the active species in the conversion to [*URE3*]. However, it appears that a conformational change might be a necessary prerequisite to allow productive interaction of the soluble protein with the growing fiber. Alternatively, newly bound molecules might have to be refolded in order to allow recruitment of further monomers from the solution. Whether our studies of a yeast protein with prion-like properties reflect mammalian PrP^{Sc} formation remains to be determined.

Comparison with other amyloid-forming protein domains

Our in vitro experiments reproduce two steps in the mechanism of amyloid formation, which appear to play an important role in human neurodegenerative diseases: release of an amyloid-forming fragment by proteolytic cleavage and autocatalytic polymerization upon addition or spontaneous formation of seed particles. Further studies on this system could not only improve our understanding of the mechanism and kinetics of amyloid formation but might also allow comparison of different amyloid-forming proteins or protein domains. For example, full-length PrP^{Sc} does not polymerize into amyloid fibrils, but PrP 27-30 generated from PrP^{Sc} by limited proteolysis does polymerize spontaneously (McKinley et al., 1991). Moreover, it has been shown that expression of GST-Sup35p in yeast can suppress the [*PSI*] prion phenotype (Dagkesamanskaia et al., 1997), but a fusion protein of GST with the prion-forming domain of Sup35p can form amyloid fibers (M.M. Balbirnie & D. Eisenberg, pers. comm., 1999). Furthermore, amyloid-like fiber formation has been shown for N-terminal parts of Huntingtin with extended polyglutamine repeats after proteolytic cleavage of GST fusion proteins (Scherzinger et al., 1997, 1999). Because other studies (DePace et al., 1998) indicate substantial similarities between yeast prion states and polyglutamine diseases, it would be interesting to examine the potential of such GST fusion proteins themselves to undergo autocatalytic polymerization as mediated by the polyglutamine domain of Huntingtin.

Materials and methods

Plasmids

For expression of the fusion protein between UPD and GST from *Schistosoma japonicum*, the N-terminal part of the URE2 gene was amplified by PCR using the primers UPD3 (GTTGTAGGATCCA TGATGAATAACAACGGCAACC) and UPD4 (TCTCGTGAAT TCATTATTGGCTACCATTGCGGC) and inserted as a BamH I/EcoR I fragment into pGEX-2T (Amersham Pharmacia Biotech, Piscataway, New Jersey) to obtain pMS50. The C-terminal moiety of the fusion protein corresponds to amino acids 1–69 of Ure2p. For expression of GST-Ure2p, pMS50 was cut with Not I/EcoR I, and a corresponding fragment from pRW530 (provided by R.B. Wickner) comprising the C-terminal part of URE2 was inserted.

Protein isolation and thrombin cleavage

Purification of the fusion proteins using glutathione Sepharose 4B (Amersham Pharmacia Biotech) was performed as proposed by the manufacturer, except that 0.2% Triton X-100 was added to the washing and elution buffers and 20 mM Tris buffers were used instead of phosphate to avoid difficulties with the negative staining procedure for electron microscopy. The purified proteins were dialyzed against TBS-TX (20 mM Tris pH 7.3, 30 mM KCl, 140 mM NaCl, 0.2% Triton X-100). Protein concentrations were determined using the BCA assay system (Pierce, Rockford, Illinois). Thrombin cleavage was performed as described in the manufacturers manual (Amersham Pharmacia Biotech). For cleavage in the presence of 20% glycerol, four times the normal amount was used to compensate for reduced activity of the protease under these conditions. Cleavage was more than 90% complete within 2 h and stopped by the addition of 1 mM PMSF after 8 h to prevent unspecific cleavage.

Antibodies

Two rabbits were immunized with the purified GST-Ure2 fusion protein. Polyclonal antiserum C8662 obtained from one of the animals showed strong and specific reactivity against GST and Ure2, either purified from *E. coli* or expressed in yeast. The UPD was detected only when an additional denaturation step was included (see below and Results).

HPLC and mass spectrometry

Reversed-phase HPLC employed a C-18 column (Vydac) of 4.6 mm $\times$ 15 cm, operating at a flow rate of 1.0 mL/min. Buffer A was H_2O/0.1% TFA, and buffer B was acetonitrile/0.08% TFA. The separation was carried out at room temperature with a linear gradient of 0–60% B over 60 min. The UV chromatogram was recorded at 214 nm. For MALDI-MS an aliquot of 0.5 μL of each HPLC fraction was mixed with 0.5 μL a-cyano-2-hydroxycinnamic acid solution (Hewlett-Packard) and dried on the target plate. The MALDI mass spectrometer was a PE Biosystem Voyager operated in linear mode without delayed extraction. ESI-MS was carried out using a PE-Sciex API-300 quadrupole mass spectrometer equipped with an electrospray ionization source. HPLC fractions were infused directly into the ESI source at 5 μL/min. Spectra accumulated for $\sim$2 min were smoothed and deconvoluted using the Biomultiview software supplied with the mass spectrometer. Mo-

lecular weights based on average atomic masses were calculated using the MacBioSpec program.

CD spectroscopy

CD spectra were collected on a JASCO 720 spectropolarimeter equipped with a stress plate modulator continuously purged with dry nitrogen using 0.1 cm cells. The concentration of GST-UPD was 10 μM in 4 mM Tris pH 7.3, 7.5 mM KCl, 28 mM NaCl, and 0.04% Triton X-100. Buffer spectra obtained under identical conditions were subtracted. Mean residue molar ellipticities were calculated based on the protein concentration, the number of residues, and the cell pathlength. The secondary structure content was calculated by deconvolution of the amide CD spectra (Sreerama & Woody, 1993).

Fourier transform infrared spectroscopy

FTIR analysis of Ure2p, UPD, and GST-UPD was carried out in TBS-TX buffer. The proteins were lyophilized from H_2O-containing buffers and reconstituted with D_2O. Soluble GST-UPD was cleared of any aggregates that may have formed by centrifugation (Eppendorf tabletop centrifuge at 14,000 $\times$ *g*) and measured immediately afterward. Ure2p, UPD, and GST-UPD fibers were measured in suspension. To obtain clear signals of the aggregated protein only, GST-UPD fibers were pelleted and resuspended in fresh TBS-TX buffer in D_2O. FTIR spectra were recorded with a Perkin-Elmer (Norwalk, Connecticut) System 2000 FTIR spectrophotometer with a microscope attachment. The samples were enclosed between two AgCl windows (International Crystal Laboratories, Garfield, New Jersey) with a pathlength of 50 μm. Spectra were recorded in the amide I′ region between 1,750 and 1,550 cm^{-1}. A blank control of buffer was used to subtract nonprotein contributions from the spectra. Spectral analysis and self-deconvolution were carried out as previously described (Byler & Susi, 1986) and modified (Wille et al., 1996).

Electron microscopy

Samples were prepared on carbon-coated 600-mesh copper grids that were glow-discharged for 30 s. Five μl aliquots were adsorbed for about 30 s and negatively stained with two drops of freshly filtered 2% ammonium molybdate or 2% uranyl acetate. Samples from sucrose gradients were washed with two drops of each 0.1 M and 0.01 M ammonium acetate prior to staining. After drying, the samples were viewed in a JEOL JEM 100CX II electron microscope at 80 kV and a standard magnification of 40,000. The magnification was calibrated with negatively stained catalase crystals.

Congo red dye binding

Protein aggregates were sedimented at 14,000 $\times$ *g* in a tabletop centrifuge (Eppendorf, Westbury, New York), washed in four volumes of phosphate buffer (100 mM sodium phosphate pH 7.4, 150 mM NaCl), and resuspended in 10 volumes of 100 mM Congo red dye in phosphate buffer. After 1.5 h of incubation at room temperature with constant end-over-end agitation, the samples were spun down again. The pellets were washed twice, once with two volumes of phosphate buffer and once with two volumes of H_2O. After the last wash, the precipitates were resuspended in 10 to 20 μl of H_2O and dried on glass slides. The dried specimens were viewed in a light microscope with polarization filters. Pictures were taken in normal illumination and with crossed polarizers.

Aggregation and thioflavine T assay

To follow formation of ordered aggregates, purified proteins were incubated in TBS-TX buffers at room temperature under constant slow rotation. Samples from aggregation experiments were diluted to 0.1 mg/mL in the presence of 5 mM ThT. Fluorescence intensity was determined on a LS 50B (Perkin-Elmer, Foster City, California) fluorimeter at 482 nm (excitation at 450 nm; excitation slit, 5 nm; emission slit, 10 nm). Due to the formation of macroscopic aggregates, individual samples showed significant variance in fluorescence intensity. To obtain reliable data, two to five measurements were taken for each sample and the average fluorescence intensity calculated.

SDS-PAGE and Western blotting

Samples for gel electrophoresis were diluted into 8 M urea to a final concentration of at least 6 M. SDS-PAGE was performed according to standard procedures. After transfer from the gel to nitrocellulose membrane (Amersham Pharmacia Biotech) according to standard protocols, the membrane was incubated for 30 min in 0.2 M NaOH, rinsed with water, and developed according to standard ECL procedures (Amersham Pharmacia Biotech). All blots were developed using the anti-GST-Ure2 antiserum described above.

Sucrose gradient centrifugation

For density analysis of aggregates, 200 μl of sample were applied to a 4 mL 15–60% linear sucrose gradient and subjected to centrifugation in a Beckman L8-M ultracentrifuge and SW60 rotor at 40,000 rpm (210,000 $\times$ *g*) for 18 h at 4 °C. For larger scale preparation of fibers, 600 μl were applied to a 12 mL gradient and subjected to centrifugation in a SW41 rotor at 33,500 rpm (210,000 $\times$ *g*) for 18 h at 4 °C. The pellet fraction was diluted fivefold into TBS-TX buffer, pelleted by centrifugation at 100,000 $\times$ *g* for 2 h, and resuspended in fresh TBS-TX buffer.

Proteinase K digestion

Proteins were incubated at concentrations of 1 mg/mL in the presence of 25 mg/mL proteinase K at 37 °C. Samples were removed at various time points and proteolysis stopped by addition of 1 mM PMSF. For samples containing 20% glycerol, the activity of the proteinase under these conditions was tested using chromozym TRY test substrate (Boehringer-Mannheim, Indianapolis, Indiana). Proteinase K (50 mg/mL) was used to compensate for reduced activity.

Acknowledgments

We are grateful to Reed B. Wickner for providing URE2 plasmids. This work was supported by a Forschungsstipendium from the Deutsche Forschungsgemeinschaft (DFG) to M. Schlumpberger and by Centeon, Inc.

References

Aguzzi A, Weissmann C. 1997. Prion research: The next frontiers. *Nature 389*:795–798.

Byler DM, Susi H. 1986. Examination of the secondary structure of proteins by deconvolved FTIR spectra. *Biopolymers 25*:469–487.

Chernoff YO, Lindquist SL, Ono B, Inge-Vechtomov SG, Liebman SW. 1995. Role of the chaperone protein Hsp104 in propagation of the yeast prion-like factor [*psi*$^+$]. *Science 268*:880–884.

Cohen AS, Shirahama T, Skinner M. 1982. Electron microscopy of amyloid. In: Harris JR, ed. *Electron microscopy of proteins*, vol. 3. New York: Academic Press. pp 165–206.

Cohen FE, Prusiner SB. 1998. Pathologic conformations of prion proteins. *Annu Rev Biochem 67*:793–819.

Coschigano PW, Magasanik B. 1991. The *URE2* gene product of *Saccharomyces cerevisiae* plays an important role in the cellular response to the nitrogen source and has homology to glutathione *S*-transferases. *Mol Cell Biol 11*:822–832.

Dagkesamanskaia AR, Kushnirov VV, Paushkin SV, Ter-Avanesian MD. 1997. Fusion of glutathione S-transferase with the N-terminus of yeast Sup35p protein inhibits its prion-like properties. *Genetika 33*:610–615.

DePace AH, Santoso A, Hillner P, Weissman JS. 1998. A critical role for amino-terminal glutamine/asparagine repeats in the formation and propagation of a yeast prion. *Cell 93*:1241–1252.

Edskes HK, Gray VT, Wickner RB. 1999. The [*URE3*] prion is an aggregated form of Ure2p that can be cured by overexpression of Ure2p fragments. *Proc Natl Acad Sci USA 96*:1498–1503.

Gajdusek DC. 1988. Transmissible and non-transmissible amyloidoses: Autocatalytic post-translational conversion of host precursor proteins to β-pleated sheet configurations. *J Neuroimmunol 20*:95–110.

Glover JR, Kowal AS, Schirmer EC, Patino MM, Liu J-J, Lindquist S. 1997. Self-seeded fibers formed by Sup35, the protein determinant of [*PSI*$^+$], a heritable prion-like factor of *S. cerevisiae*. *Cell 89*:811–819.

Jarrett JT, Lansbury PT Jr. 1993. Seeding "one-dimensional crystallization" of amyloid: A pathogenic mechanism in Alzheimer's disease and scrapie? *Cell 73*:1055–1058.

King C-Y, Tittman P, Gross H, Gebert R, Aebi M, Wüthrich K. 1997. Prion-inducing domain 2-114 of yeast Sup35 protein transforms *in vitro* into amyloid-like filaments. *Proc Natl Acad Sci USA 94*:6618–6622.

Kushnirov VV, Ter-Avanesyan MD. 1998. Structure and replication of yeast prions. *Cell 94*:13–16.

LeVine H. 1993. Thioflavine T interaction with synthetic Alzheimer's disease β-amyloid peptides: Detection of amyloid aggregation in solution. *Protein Sci 2*:404–410.

Liebman SW, Derkatch IL. 1999. The yeast [*PSI*$^+$] prion: Making sense of nonsense. *J Biol Chem 274*:1181–1184.

Lindquist S. 1997. Mad cow meet psi-chotic yeast: The expansion of the prion hypothesis. *Cell 89*:495–498.

Masison DC, Maddelein M-L, Wickner RB. 1997. The prion model for [*URE3*] of yeast: Spontaneous generation and requirements for propagation. *Proc Natl Acad Sci USA 94*:12503–12508.

Masison DC, Wickner RB. 1995. Prion-inducing domain of yeast Ure2p and protease resistance of Ure2p in prion-containing cells. *Science 270*:93–95.

McKinley MP, Meyer RK, Kenaga L, Rahbar F, Cotter R, Serban A, Prusiner SB. 1991. Scrapie prion rod formation *in vitro* requires both detergent extraction and limited proteolysis. *J Virol 65*:1340–1351.

McTigue MA, Williams DR, Tainer JA. 1995. Crystal structures of a schistosomal drug and vaccine target: Glutathione S-transferase from *Schistosoma japonica* and its complex with the leading antischistosomal drug Praziquantel. *J Bol Biol 246*:21–27.

Newnam GP, Wegrzyn RD, Lindquist SL, Chernoff YO. 1999. Antagonistic interactions between yeast chaperones Hsp104 and Hsp70 in prion curing. *Mol Cell Biol 19*:1325–1333.

Patino MM, Liu J-J, Glover JR, Lindquist S. 1996. Support for the prion hypothesis for inheritance of a phenotypic trait in yeast. *Science 273*:622–626.

Paushkin SV, Kushnirov VV, Smirnov VN, Ter-Avanesyan MD. 1996. Propagation of the yeast prion-like [*psi*$^+$] determinant is mediated by oligomerization of the *SUP35*-encoded polypeptide chain release factor. *EMBO J 15*:3127–3134.

Paushkin SV, Kushnirov VV, Smirnov VN, Ter-Avanesyan MD. 1997. In vitro propagation of the prion-like state of yeast Sup35 protein. *Science 277*:381–383.

Perrett S, Freeman SJ, Butler PJG, Fersht AR. 1999. Equilibrium folding properties of the yeast prion protein determinant Ure2. *J Mol Biol 290*:331–345.

Prusiner SB. 1982. Novel proteinaceous infectious particles cause scrapie. *Science 216*:136–144.

Prusiner SB. 1998. Prions. *Proc Natl Acad Sci USA 95*:13363–13383.

Prusiner SB, McKinley MP, Bowman KA, Bolton DC, Bendheim PE, Groth DF, Glenner GG. 1983. Scrapie prions aggregate to form amyloid-like birefringent rods. *Cell 35*:349–358.

Scherzinger E, Lurz R, Turmaine M, Mangiarini L, Hollenbach B, Hasenbank R, Bates GP, Davies SW, Lehrach H, Wanker EE. 1997. Huntingtin-encoded polyglutamine expansions form amyloid-like protein aggregates in vitro and in vivo. *Cell 90*:549–558.

Scherzinger E, Sittler A, Schweiger K, Heiser V, Lurz R, Hasenbank R, Bates GP, Lehrach H, Wanker EE. 1999. Self-assembly of polyglutamine-containing huntingtin fragments into amyloid-like fibrils: Implications for Huntington's disease pathology. *Proc Natl Acad Sci USA 96*:4604–4609.

Sreerama N, Woody RW. 1993. A self-consistent method for the analysis of protein secondary structure from circular dichroism. *Anal Biochem 209*: 32–44.

Sunde M, Blake CCF. 1998. From the globular to the fibrous state: Protein structure and structural conversion in amyloid formation. *Q Rev Biophys 31*:1–39.

Tatzelt J, Prusiner SB, Welch WJ. 1996. Chemical chaperones interfere with the formation of scrapie prion protein. *EMBO J 15*:6363–6373.

Taylor KL, Cheng N, Williams RW, Steven AC, Wickner RB. 1999. Prion domain initiation of amyloid formation in vitro from native Ure2p. *Science 283*:1339–1343.

Ter-Avanesyan MD, Kushnirov VV, Dagkesamanskaya AR, Didichenko SA, Chernoff YO, Inge-Vechtomov SG, Smirnov VN. 1993. Deletion analysis of the SUP35 gene of the yeast *Saccharomyces cerevisiae* reveals two non-overlapping functional regions in the encoded protein. *Mol Microbiol 7*:683–692.

Thual G, Komar AA, Bousset L, Fernandez-Bellot E, Cullin C, Melki R. 1999. Structural characterization of *Saccharomyces cerevisiae* prion-like protein Ure2. *J Biol Chem 274*:13666–13674.

Wickner RB. 1994. [*URE3*] as an altered URE2 protein: Evidence for a prion analog in *Saccharomyces cerevisiae*. *Science 264*:566–569.

Wickner RB, Masison DC. 1996. Evidence for two prions in yeast: [*URE3*] and [*PSI*]. *Curr Top Microbiol Immunol 207*:147–160.

Wille H, Zhang G-F, Baldwin MA, Cohen FE, Prusiner SB. 1996. Separation of scrapie prion infectivity from PrP amyloid polymers. *J Mol Biol 259*:608–621.